Energy scales of the excitations associated with superconductivity: an analysis of the infrared and visible in-plane response of $Bi_2Sr_2CaCu_2O_{8+\delta}$

A. F. Santander-Syro[a], R. P. S. M. Lobo[a], N. Bontemps[a],
Z. Konstantinovic[b], Z. Z. Li[b], and H. Raffy[b]

[a]Laboratoire de Physique du Solide, Ecole Supérieure de Physique et Chimie Industrielles de la Ville de Paris, CNRS UPR 5, 75231 Paris cedex 5, France
[b]Laboratoire de Physique des Solides, Université Paris-Sud 91405 Orsay cedex, France

ABSTRACT

The *ab*-plane infrared and visible (3 meV–3 eV) response of $Bi_2Sr_2CaCu_2O_{8+\delta}$ (Bi-2212) thin films (prepared by r.f. sputtering on $SrTiO_3$) has been measured between 300 K and 10 K for different doping levels. In the superconducting state, dramatic differences appear between the underdoped and overdoped regimes regarding the electrodynamics of the formation of the superfluid condensate. In the over-doped regime, the superfluid grows up by removing states from energies below 60 meV. This energy is of the order of a few times the superconducting gap. In this respect, overdoped Bi-2212 exhibits a conventional behavior. In the underdoped regime, states extending up to 2 eV contribute to the superfluid. This anomalously large energy scale may be assigned to a change of electronic kinetic energy at the superconducting transition, and is compatible with an electronic pairing mechanism.

Keywords: Infrared spectroscopy, superconductivity, cuprates, highly-correlated electron systems.

1. INTRODUCTION

Two phenomena essential in the physics of superconducting materials are common to conventional and cuprate superconductors: the binding of quasi-particles (QP) into Cooper pairs and the appearance of global phase coherence betweeen pairs. This results into the formation of a superfluid condensate. However, while these phenomena are well understood in the case of conventional metals, how QP binding and phase coherence are actually realized in cuprates is a central problem in high-T_c superconductivity. In order to grasp a clue about the mechanism of high T_c superconductivity in cuprates, one key issue is the energy scale of excitations responsible for pairing. This question can be addressed in infrared (IR) and visible spectroscopy, by investigating the spectral weight W, *i.e.* the area under the real part of the optical conductivity (related, in simple terms, to the ratio n/m where n is the carrier density and m their mass):[1,2]

$$W = \int_{0^+}^{\omega_c} \sigma_1(\omega, T) d\omega, \tag{1}$$

where $\sigma_1(\omega, T)$ is the frequency (ω) and temperature (T) dependent conductivity, and ω_c is a cut-off frequency. The Ferrell-Glover-Tinkham (FGT) sum rule[3,4] requires that the spectral weight ΔW lost when decreasing the temperature from the normal state into the superconducting state, must be retrieved in the spectral weight W_s of the $\delta(\omega)$ function centered at zero frequency, which represents the superfluid condensate. The sum rule is exact if integrating up to infinity, and results from charge conservation. Actually the sum rule is exhausted ($\Delta W \simeq W_s$) provided the integration is performed up to a large enough value $\hbar\Omega_M$. In conventional superconductors, $\hbar\Omega_M \sim 16 k_B T_c$, or $\sim 4\Delta$ (Δ is the superconducting gap).[3,4] $\hbar\Omega_M$ is considered to be a typical energy of the boson spectrum responsible for the pairing mechanism. Would cuprates display this

Send correspondence to NB (e-mail: Nicole.Bontemps@espci.fr). AFSS present address: University of Illinois at Chicago, Dept. of Physics, 845 W. Taylor St., Chicago IL 60607, USA.

Proceedings of SPIE Vol. 4811 Superconducting and Related Oxides: Physics and Nanoengineering V, edited by Ivan Bozovic and Davor Pavuna (SPIE, Bellingham, WA, 2002) © 2002 SPIE · 0277-786X/02/$15.00

conventional behavior, then taking a typical maximum gap magnitude (in a d-wave superconductor) Δ_M of 25 meV yields $\hbar\Omega_M \sim 0.1$ eV.[5,6] An apparent violation of the sum rule, i.e. $\Delta W < W_s$ when integrating up to 0.1 eV was observed from interlayer conductivity data: exhausting the sum rule could then require an anomalously large energy scale, which was suggested to be related to a change of interlayer kinetic energy when the superfluid builds up.[7–9] This was contrasted with conventional *in-plane* energetics.[7] Nevertheless, a decrease of the *in-plane* kinetic energy, suggested long ago as a possible pairing mechanism in the framework of the hole undressing scenario,[10,11] was given renewed interest.[12–14] Lately, ellipsometric measurements combined with IR reflectivity showed that in-plane spectral weight was lost in the visible range, but without direct evidence that this spectral weight is indeed transferred into the condensate.[15]

The data reported in this paper show that an electronic energy is relevant to the pairing mechanism. We carefully selected three thin films from the Bi-2212 family probing three typical locations in the phase diagram: the underdoped (UND), the optimally doped (OPT) and the overdoped (OVR) regime. A detailed study of the spectral weight changes as the temperature goes from well above T_c down to $T \ll T_c$ allows to work out the FGT sum rule with well controlled error bars. We find that within these error bars, retrieving the condensate spectral weight in the OVR and OPD samples requires integrating up to an energy of the order of 0.1 eV (800 cm^{-1}), *i.e.* a conventional energy scale. In the UND sample, the integration must be performed up to at least 16000 cm^{-1} (2 eV), an energy scale much larger than typical boson energies in a solid. We derive the associated change of the in-plane kinetic energy, which turns out to agree with some theoretical calculations.[12,13,16]

The paper is divided as follows: after a description of the sample fabrication, characterization and selection, and the experimental set-up (section 2), we will show the experimental results (section 3). Then, in section 4, we will present the analysis of the data in terms of the spectral weight and the behavior of a partial FGT sum rule as a function of the cut-off frequency. We will give an interpretation of the results in terms of a change of the in-plane kinetic energy. The paper will close with some concluding remarks.

2. SAMPLES AND MEASUREMENTS

The thin films studied in this work were epitaxially grown by r.f. magnetron sputtering on (100) $SrTiO_3$ substrates heated at temperatures $\gtrsim 700°C$.[17,18] X-ray analyses confirmed that the films are single phase, with the *c*-axis perpendicular to the substrate.[19] Their maximum critical temperature (defined at zero resistance) is ~ 84 K. The **a** and **b** axes show a single orientation (45° with respect to the substrate axes), with possible exchanges between **a** and **b** from one grain to another. The directions -Cu-O-Cu- are parallel to the (100) and (010) axes of the substrate. The films may be under- or over-doped just by ex-situ oxygen anealing within a larger doping range than single crystals.

In total, thirteen samples of Bi-2212 thin films were studied for this work. The films prepared by the above procedure are usually in a nearly optimally doped state. The various doping levels (UND and OVR) were obtained by post-annealing the films in a controlled atmosphere.[18] All the films were characterized by electrical resistance measurements, and a first estimate of their thicknesses was obtained by Rutherford Back-Scattering (RBS) on samples prepared under exactly the same conditions as the ones used in this work. Their optical homogeneity in the mid-infrared was characterized by infrared microscopy (μIR), as will be described shortly. Observed by standard optical microscopy, the films are smooth and homogeneous up to a magnifying power of 200. The full infrared-visible reflectivities, taken at typically 15 temperatures between 10 K and 300 K and at quasi-normal incidence (electric field $\parallel$ *ab*-plane within less than 10 degrees), were measured for all the films. Reflectivities were measured in the spectral range $[30 - 7000]$ cm^{-1} with a Bruker IFS-66v Fourier Transform spectrometer, supplemented with standard grating spectroscopy in the range $[4000 - 28000]$ cm^{-1} (Cary-5). Our cryogenic measurements were done in a home-built helium-flux cryostat, with a sample holder immersed in the helium gas flow. The temperature in our set-up can be stabilized within 0.2 K.

To determine of the absolute value of the reflectivity, we used as unity reflectivity references a golden mirror in the $30-7000$ cm^{-1} spectral range, and a silver mirror in the remaining spectral range. Our sample holder was designed to allow to commute at each temperature, between the reference and the sample, placing one or the other at the same place on the optical path within an angular accuracy better than 10^{-3} rad. A circular aperture placed in front of the sample/reference position guarantees that the same flux is irradiating the sample and the

reference. The temperature of the sample/reference block is measured independently of that of the helium gas flow. Once thermal equilibrium has been achieved in the entire cryogenic set-up, consecutive measurements of the sample and reference spectra can be done, under exactly the same conditions. With this set-up, and using thin films whose surface (typically 6×6 mm^2) is easily ten times larger than standard single crystals, we can measure *relative* variations in the reflectivity within less than 0.2%, even in the visible range. We were thus able to monitor the temperature evolution of the reflectivity spectra in the full available range (30-28000 cm^{-1}). It is known indeed that temperature changes of the optical response of cuprates in the mid-infrared and the visible ranges are small, but cannot be neglected.[20] They are obviously important if one is looking for a spectral weight transfer originating from (or going to) any part of the *whole* frequency range. Yet, as remarked by van der Marel and coworkers,[21] most studies rely on a single spectrum at one temperature in the visible. Our accuracy in the determination of the *absolute* reflectivity is ± 1 %.

Even if the infrared spectroscopy measures the bulk optical properties of cuprates (the infrared skin-depth of Bi-2212 is $\gtrsim 3000$ Å), a flat surface of high optical quality *in the whole measured spectral range* is an important requirement for the accuracy in the measurement of the *absolute* value of the reflectivity. We thus characterized the *mid-infrared* surface flatness and optical quality of our films by infrared microscopy at room temperature, using the infrared microscope of the MIRAGE beamline at LURE (Orsay).[22] In this microscope, the light being focalised on a point on the sample has been previously analyzed by a Fourier Transform spectrometer. In this way, the infrared reflectivity spectrum for each measured point is available. In our case, we worked at a spatial resolution of 20 μm. We then made, for each sample, spatial scans over areas typically 160×160 μm^2, recording for each measured point the spectrum in the $[500 - 4000]$ cm^{-1} range.

Figure 1 illustrates the cases of a good (left) and a bad (right) quality sample in the mid-infrared [the figure on the right corresponds actually to a thin film of $YBa_2Cu_3O_{7-\delta}$ (YBCO-7), with a $T_c = 90$ K]. We found that, in general terms, a defect whose size is comparable to the infrared wavelenghts ($\gtrsim 10$ μm), and that is easily spotted with the visible microscope (picture in Fig. 1, right), can extremelly perturb the local reflectivity spectra. (We have not, on the other hand, found any case were a smooth region in the optical microscope was defective under the infrared microscope). If the ensemble of these infrared-defective regions represents a few percent of the total sample surface, then the *average* reflectivity of the whole surface will not accurately represent the *intrinsic* value of the absolute reflectivity of the sample (*i.e.*, the average reflectivity over the whole surface will differ by more than 1% from the actual value of the reflectivity one would obtain with a surface defectiveless sample of the same doping characteristics). Our characterisations show as well that the infrared spectra are not sensitive to sub-micronic defects, whose size is comparable to the wavelengths in the visible (Fig. 1, left).

A first screening of the samples was then done based on their resistive, optical-microscopy and μIR characteristics. We selected the samples showing a metallic behavior in the normal state, having the narrower transitions (~ 20 K to ~ 10 K for UND to OVR, respectively), not showing scratches, defects or inhomogeneities under the optical microscope, and having homogeneous μIR charts. The reflectivity spectra of the samples thus selected were adjusted to obtain their conductivities, using a fitting procedure that will be discussed in the next section. In this fitting procedure, the thickness of the sample enters as a parameter. Samples whose measured thickness differed by more than 15% (the accuracy of RBS measurements on Bi-2212) from the thickness needed to adjust the measured reflectivity were discarded. Samples showing abnormal electronic behaviour (*e.g.*, localized states at low frequency, or a temperature dependence of the low-frequency conductivity not matching the DC measurements) were discarded as well. At the end, three samples having passed confidently all the screenings, and spanning the three different doping regions, were selected for a thorough analysis. The critical temperatures (doping) of the selected films are 70 K (UND), 80 K (OPT) and 63 K (OVR). In the remaining of the paper, we will refer to these samples as B70KUND, B80KOPT and B63KOVR, respectively.

The thicknesses of the B80KOPT and B63KOVR samples were verified by a second run of RBS measurements after the optical measurements, yielding 395 nm and 270 nm (± 30 nm) respectively, in agreement with the thicknesses derived from the fits to their reflectivities. For the underdoped sample, in an attempt to achieve a better accuracy on the thickness, we glued the suface of two halves of the film and imaged a slice by TEM. However we eventually did not improve the accuracy, with respect to the first indirect measurement on a film

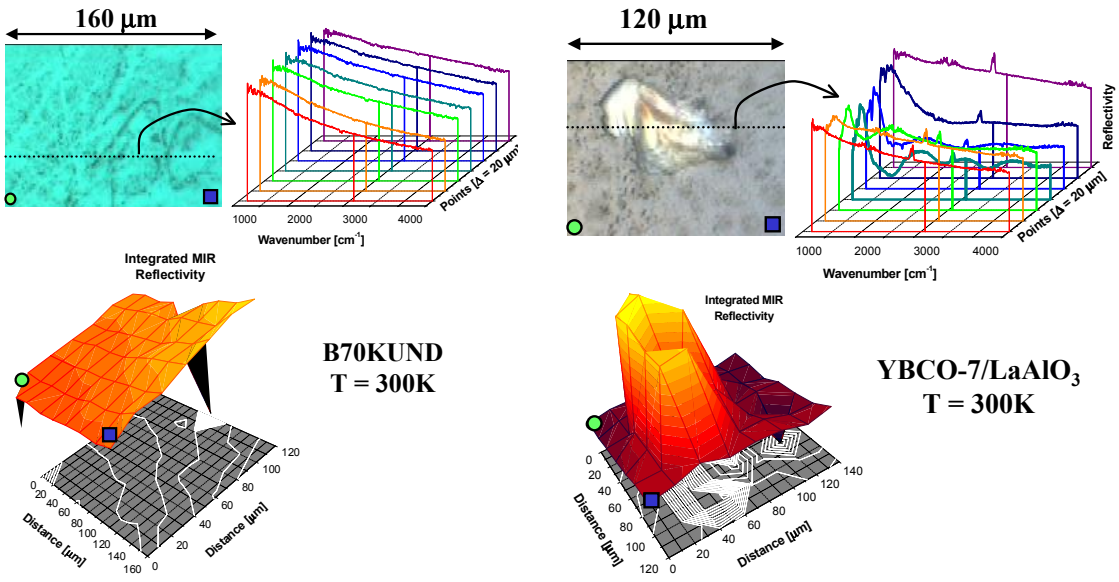

Figure 1. Left panel: infrared chart of the B70KUND sample. The picture of the scanned region (upper left corner) shows some sub-micronic defects. The reflectivity spectra (upper right corner) along the dotted line are identical, and the integrated reflectivity chart (lower left corner) is homogeneous. (The two peaks correspond to mechanical instabilities in the microscope sample holder during the measurements, and can not be reproduced). Right panel: infrared chart of a YBCO-7 sample, displaying surface defects larger than 10 μm. Note that the reflectivity spectra along the dotted line, and the integrated reflectivity chart both show accidents clearly correlated with the surface defect seen on the picture.

grown under the same conditions (but on a MgO substrate) which yielded 220 nm. This is in agreement within 10% with the thickness from the fit.

Figure 2 shows the resistance of the three selected samples, and the DC values obtained from the optical data (see next section).

3. EXPERIMENTAL RESULTS

3.1. Raw data

Figure 3-(a) shows two reflectivity curves (at $T = 250$ K and $T = 10$ K) of the B70KUND sample. This is an example of the typical spectra we have measured. The signal-to-noise ratio is unprecedented, and relative variations of the reflectivity of the order of 0.2% can be measured. In the far-infrared (see the inset), the three phonon peaks coming from the underlying substrate are clearly visible, specially at high temperatures (or low doping), when the system is less metallic. The lowest-energy of these peaks is the soft mode of $SrTiO_3$. We experimentally determined the optical constants of the $SrTiO_3$ at each temperature, so as to take into account the changes in reflectivity due to changes in the substrate optical properties alone. This is important when extracting the intrinsic optical constants of Bi-2212 (the procedure will be described below).

While the major temperature changes in the reflectivity occur at low frequency, where reflectivity increases with increasing doping or decreasing T, changes in the visible range are important as well. This is illustrated for the B70KUND and B63KOVR samples in Fig. 3-(b). This figure shows indeed that, in the visible range, a decrease in doping has the same qualitative effect that increasing the temperature: in both cases, the reflectivity in the visible range increases. These opposite temperature behaviors of the infrared and visible reflectivities have also been observed by temperature-modulated differential spectroscopy measurements.[23,24] The broad oscillations in the visible range spectrum come from both interband transitions and interferences of the light bouncing back and forth inside the film. The period of these oscillations, and the shape of the reflectivity in the vicinity of the plasma edge, depend on the sample thickness.

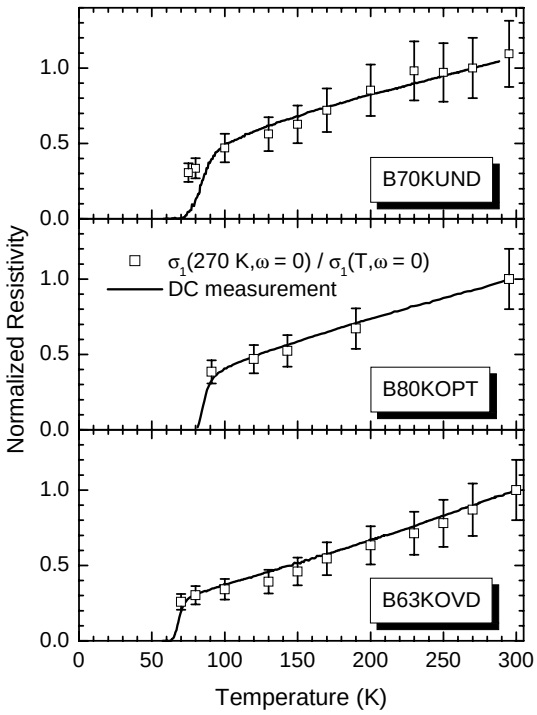

Figure 2. Measured resistance of the three selected samples (normalised to unity at high temperatures), and comparison with the DC extrapolation of the respective conductivities obtained from the reflectivity spectra.

The right panels of Fig. 3 show the reflectivities of the three samples, for a restricted set of temperatures, up to 1500 cm^{-1}. Note that, upon increasing doping, the reflectivity increases for a given temperature in this spectral range, as a consequence of the material becoming more metallic. For all matters to follow, the behavior of the optimally doped sample is intermediate between that of the underdoped and overdoped samples. We will thus, for sake of clarity and compactness in the discussion, not reconsider this sample until the end of the paper.

3.2. Extraction of the optical functions

The contributions of the substrate to the measured reflectivities preclude the Kramers-Kronig analysis on thin films. In order to extract the optical functions intrinsic to Bi-2212, we simulated its dielectric function at each temperature and doping levels using Drude-Lorentz oscillators (thus warranting causality). In the superconducting state, where a superfluid exists, we used a London oscillator as well, which is indeed necessary to simulate properly the enhancement in the reflectivity observed at low frequencies (below 500 cm^{-1}) and low temperatures (Fig. 3, right panels). We then modelled the reflectance of the film on top of a substrate, using the optical constants of $SrTiO_3$ that, as already stated, were experimentally determined for each temperature. Finally, we adjusted the attempt dielectric function of the Bi-2212 in order to fit within ± 0.5 % the raw reflectivity spectra. We found that the best description of our data was obtained by assuming an infinitely thick substrate (*i.e.*, negligible backward reflection from the rear of the substrate). Examples of such fits, for the B70KUND sample, are shown in Fig. 4 at far-infrared (left panel) and visible (right panel) frequencies. Once the dielectric function is known, we can generate any other optical function, in particular the optical conductivity.

We have calculated that, at low frequencies (where the reflectivity is close to unity), a relative error $\Delta R/R$ in the fit yields a relative error magnified by a factor 10 in the real part of the optical conductivity, provided that $\Delta R/R \ll 1$. At high frequencies (low reflectivities), the relative errors in the fit and in the optical conductivity are of the same order of magnitude. These relative errors spread over twice the range where the deviation to the

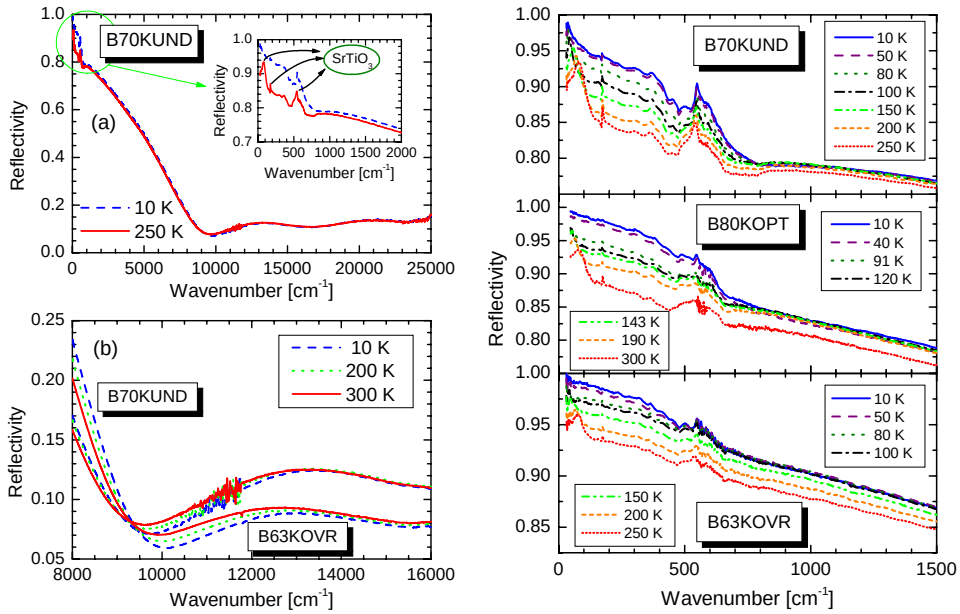

Figure 3. (a) Reflectivity of the B70KUND sample in the whole experimental range, at high (250 K) and low (10 K) temperatures. The inset shows the variation of the reflectivity in the far-infrared, and the phonon peaks from the substrate. (b) Temperature changes of reflectivity in the visible range for the B70KUND and B63KOVR samples. Right panels: reflectivity of the three samples, for a restricted set of temperatures, up to 1500 cm^{-1}.

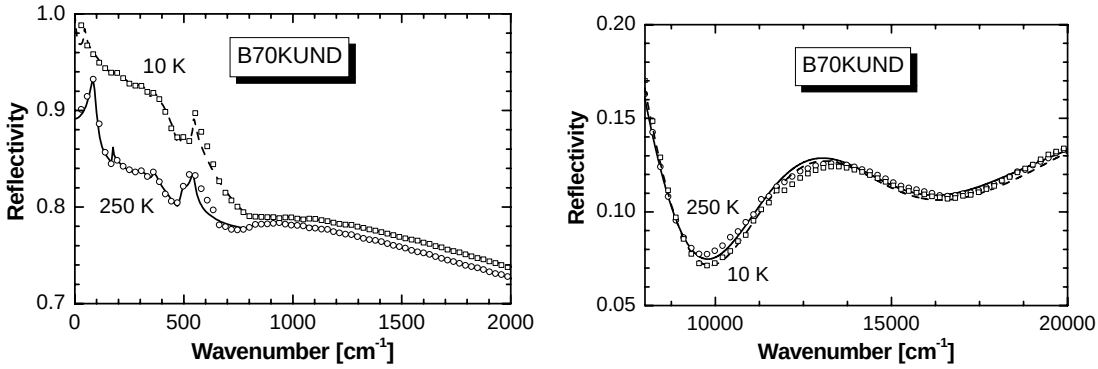

Figure 4. Measured reflectivity spectra of the B70KUND sample at 250 K and 10 K (open symbols) and fitted spectra (lines) at far-infrared (left panel) and visible (right panel) frequencies. The fits lie within ±0.5% of the raw data in the full spectral range (up to 25000 cm^{-1}), except at 620 ± 50 cm^{-1} and 13000 ± 1000 cm^{-1}, where the relative deviations are 1% and 4% respectively.

raw data occurs. The thicknesses of the films are also determined by the fit. Fits are accurate within less than 0.5% taking 241, 434 and 297 nm for the B70KUND, B80KOPT and B63KOVR samples respectively. These values differ by less than 10% from the RBS data. We checked that the associated error in the conductivity, within the experimentally measured range, is then less than 10%. The fit yields a valuable extrapolation of the conductivity in the low-energy range ($\hbar\omega < 30$ cm^{-1}, not available experimentally),[25] which is important in the evaluation of the spectral weight. In this latter range, the relative error in the conductivity reaches 20%.[26]

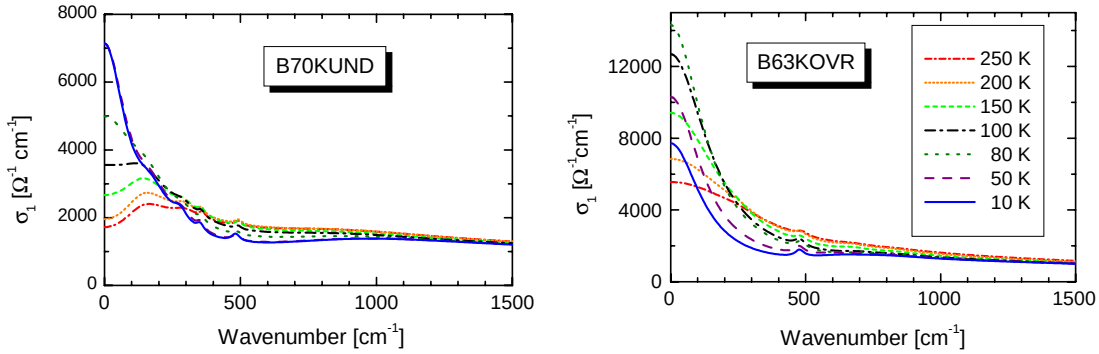

Figure 5. Selection of conductivity spectra for the B70KUND (left) and B63KOVR (right) samples. For the B70KUND sample, within the showed spectral range, the spectra at 50 K and 10 K are indistinguishable. The error bars in the conductivity spectra are $\Delta\sigma/\sigma \lesssim 10\%$ for $\hbar\omega > 30$ cm^{-1}, and $\Delta\sigma/\sigma \sim 20\%$ for $\hbar\omega < 30$ cm^{-1}.

3.3. Optical conductivities

Figure 5 shows the conductivity spectra for the B70KUND and B63KOVR samples, for the same temperatures and in the same spectral range than the reflectivity spectra of Fig. 3. Note that the conductivity values are larger for the overdoped sample, in agreement with a larger density of charge carriers. The low-frequency values of the conductivity are reasonable figures for Bi-2212: at 250 K, for example, our DC extrapolations give resistivities $\rho_{ab} \approx 500$ $\mu\Omega$-cm for the underdoped sample, and $\rho_{ab} \approx 160$ $\mu\Omega$-cm for the overdoped one. Furthermore, as can be seen in Fig. 2, the temperature behavior of the DC extrapolations is in agreement with the resistance measurements. This is remarkable, given the large ($\sim 20\%$) expected error bars in the extrapolated conductivity. In particular, for the underdoped sample, the two measurement points within the resistive transition follow quite well the trend of the measured resistance, even if the London oscillator used for our fits was only "turned-on" at $T < T_c$. Thus, whatever the phenomenon causing the large resistive transition, it is well reproduced by the extrapolations of our conductivity curves.

In the normal state, the conductivity spectra of B70KUND and B63KOVR samples are qualitatively similar. The low-frequency conductivity ($\hbar\omega \lesssim 200$ cm^{-1}) increases when the temperature decreases (metallic behavior), while at higher frequencies, because of the conservation of the spectral weight, the conductivity decreases when the temperature drops. Actually, at low frequencies the spectral weight increases rapidly when the temperature decreases down to T_c, and the conservation of the spectral weight in the normal state is retrieved upon integration up to ~ 3 eV. The implications of this observation on the electrodynamics of the normal state have already been analyzed.[26]

The superconducting transition is marked, for the overdoped sample, by a decrease of the conductivity over the spectral range shown in Fig. 5. A clear loss of spectral weight, associated with the formation of the zero-frequency condensate, is observed. In contrast, the low-frequency ($\hbar\omega \lesssim 100$ cm^{-1}) conductivity of the underdoped sample does not decrease when temperature decreases below T_c. Beyond this energy scale, the normal- and superconducting-state conductivities cross, and there is no a clear loss of spectral weight within the spectral range shown in the figure. A more detailed analysis is needed in this case, based on the FGT sum rule.

4. ANALYSIS AND INTERPRETATION

4.1. In-plane FGT sum rule for Bi-2212

Let us define $T_A \geq T_c$, and $T_B < T_c$. From an experimental point of view, the FGT sum rule compares the change in spectral weight $\Delta W = W(T_A) - W(T_B)$ (Eq. 1) and the supefluid weight W_s. For the three samples under consideration, the superfluid weight was determined for $T < T_c$ at low frequencies, within the measured

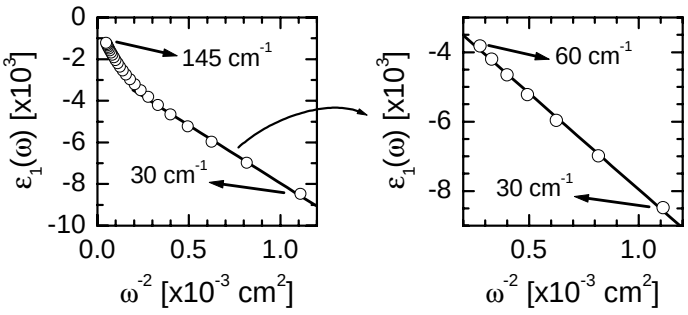

Figure 6. Determination of the superfluid spectral weight for the B70KUND sample at 10 K from the low-frequency behavior of $\epsilon_1(\omega)$. In the experimental spectral range $30 - 60$ cm^{-1}, $\epsilon_1 \sim \omega^{-2}$, so that its slope gives directly the superfluid weight.

spectral range, by looking at the region where the real part of the dielectric function $\epsilon_1(\omega)$ behaves linearly when plotted versus $1/\omega^2$ (London approximation). An example, for the B70KUND sample, is shown in Fig. 6.

The slope is directly related to the superfluid spectral weight W_s through the "London" frequency $\Omega_L = c/\lambda_L$, where λ_L is the London penetration depth. At 10 K, for instance, we find $\lambda_L = 7115$ Å, 2900 Å and 2250 Å for the B70KUND, B80KOPT and B63KOVR samples respectively. The values for the overdoped and optimally doped samples are in fair agrement with those reported in the literature.[27] There are no reliable data on the absolute value of the London penetration depth for underdoped samples.[28]

Figure 7 shows the ratio $\Delta W/W_s$ for the three samples reported in this work. In the underdoped sample, we find that at energies as large as 1 eV (8000 cm^{-1}) $\Delta W/W_s \sim 0.65 \pm 0.18$ (details about the evaluation of the error bars will be given below). It approaches 1 within the error bars at ~ 16000 cm^{-1}. A large part (~ 30 %) of the supefluid weight in the underdoped regime thus builds up at the expense of spectral weight coming from high energy regions of the optical spectrum ($\hbar\omega \geq 1$ eV). Because of our error bars, we cannot make a similar statement for the optimally doped and overdoped samples, where the sum rule may be exhausted at roughly $500 - 1000$ cm^{-1}. Our results for the optimally doped and overdoped samples thus do not contradict earlier similar work in YBCO-7 and $Tl_2Ba_2CuO_{6+\delta}$ (Tl-2212).[9] Underdoped YBCO-7 showed a conventional behavior, possibly because only one spectrum is usually recorded in the visible range, which is precisely the energy range that matters in this case.[21] On the other hand, our results in the underdoped regime are in agreement with recent ellipsometric measurements in the visible range, combined with IR reflectivity, which show that in-plane spectral weight is lost in the visible range.[15] However, these results did not provide direct evidence that this spectral weight is indeed transferred into the condensate.

The remarkable behavior of the underdoped sample must be critically examined in light of the uncertainties that enter in the determination of the ratio $\Delta W/W_s$. The determination of ΔW assumes that $W(T_A)$ is a fair estimate of the spectral weight obtained at $T_B < T_c$, defined as $W_n(T_B)$, *if the system could be driven normal at that temperature*. While this assumption is correct in BCS superconductors, it may no longer be valid for high-T_c superconductors.[29] Hence, our taking the normal-state spectral weight $W(T_A \geq T_c)$ instead of $W_n(T_B)$ (unknown) may bias the sum rule.

The error incurred by doing so can be estimated as follows. Figure 8 displays the temperature dependence, from 300 K down to 10 K, of the relative spectral weight $W(\omega_c, T)/W(\omega_c, 300\text{K})$, for three selected integration ranges, according to Eq. 1. At $\omega_c = 1000$ cm^{-1}, the normalized spectral weight exhibits a significant increase as the temperature is lowered, and could therefore keep changing in the superconducting state. Hence $W(T_A)$ is most likely to give too small an estimate for $W_n(T_B)$ at $T < T_c$, in this energy range. In the case of the underdoped sample, and below 5000 cm^{-1}, we extrapolated the data from $T \gtrsim T_c$ in Fig. 8, so as to maximize the error in $W_n(T_B)$. Such estimates have been performed for a number of cut-off frequencies starting from 100 cm^{-1}, showing that this error is the largest at low frequencies and becomes negligible starting from 5000 cm^{-1}. At 20000 cm^{-1}, the spectral weight is constant, meaning that the redistribution of spectral weight lies within this

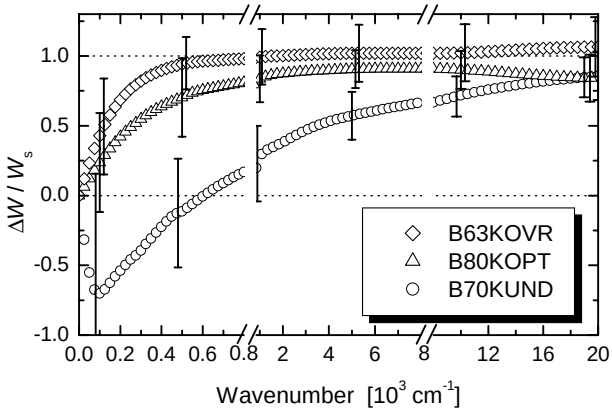

Figure 7. Ratio $\Delta W/W_s$ versus frequency showing the exhaustion of the FGT sum rule at conventional energies for the OVR (diamonds, right error bars) and OPT (triangles, middle error bars) samples. An unconventional ($\sim$ 16000 cm^{-1} or 2 eV) energy scale is required for the UND sample (circles, left error bars). Note that the frequency scale changes at 800 and 8000 cm^{-1}.

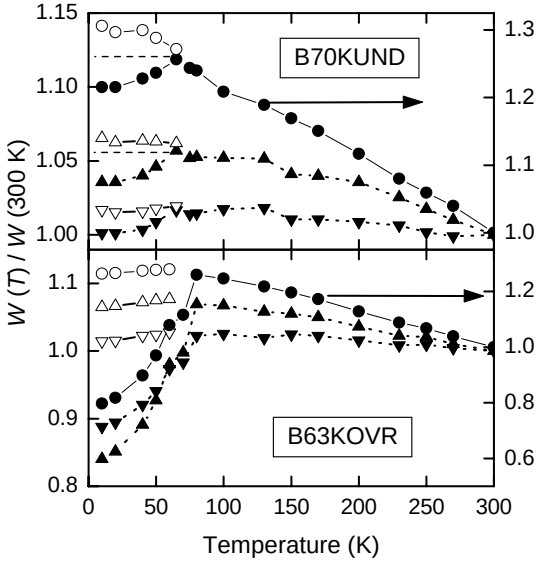

Figure 8. Effective spectral weight $W(T,\omega_c)/W(300\text{K},\omega_c)$ versus temperature for the underdoped (top panel) and overdoped (bottom panel) samples, at different cutoff frequencies ω_c (full symbols). $\omega_c = 1000$ cm^{-1} (circles); 5000 cm^{-1} (up triangles); and 20000 cm^{-1} (down triangles). Open symbols are obtained by adding the superfluid weight $W_s(T)$ to the spectral weight $W(T < T_c)$. The dotted lines in the top panel show approximately the expected location of the open symbols if all the spectral weight was removed from low energy states (see text).

range. Above 5000 cm^{-1}, the uncertainties that we have to deal with are those due to the error in the relative change of the measured reflectivity with temperature (the error in the absolute value being irrelevant); to the fitting accuracy; and to the determination of W_s. The latter two uncertainties are not independent and must be calculated self-consistently. They yield an upper bound of 15 %–20 % in the uncertainty on the evaluation of $\Delta W/W_s$, for all frequencies. *All* uncertainties are then represented by the error bars in Fig. 7. Therefore, the top of the error bars delineates the upper limit for the FGT sum rule at each frequency.

For the underdoped sample, the violation of the sum rule, with $\Delta W/W_s = 0.65 \pm 0.18$ at 8000 cm^{-1}, is clearly established. Within the error bars, the sum rule is exhausted in this sample above 16000 cm^{-1}. The fact

that the superfluid involves high energy states is compatible with the plot below T_c of the sum of the spectral weight at finite frequency and the superfluid weight (open symbols in Fig. 8). Unlike the overdoped sample, where at 1000 cm^{-1} the spectral weight of the condensate already balances the spectral weight lost up to this frequency, in the UD sample the superfluid spectral weight exceeds the loss at 1000 cm^{-1} (by roughly a factor of 2). This corresponds to $\Delta W/W_s$ being of order 50 % at this energy, consistent with our data including the error bars (Fig. 7). At 5000 cm^{-1}, $\Delta W/W_s \sim 0.6 \pm 0.2$, and the open symbols are consistently above the normal state spectral weight, suggesting that there is still some spectral weight coming from higher energy.

4.2. Violation of the sum-rule, change of kinetic energy and pairing mechanism

One interpretation of the sum rule violation can be made in the context of the tight-binding Hubbard model. The relation between the low-frequency spectral weight and the kinetic energy E_{kin} per copper site is:[21]

$$\frac{\Delta W}{W_s} - \frac{4\pi c}{137\hbar}\frac{a^2}{V}\frac{1}{\Omega_L^2}(E_{kin,s} - E_{kin,n}) = 1 \tag{2}$$

where a is the (average) lattice spacing in the plane and V is the volume per site (SI units). This relation means that a breakdown of the FGT sum-rule up to an energy $\hbar\omega_c$ of the order of the plasma frequency (~ 1 eV for Bi-2212) is related to a change in the carrier kinetic energy $\Delta E_k = E_{kin,s} - E_{kin,n}$, when entering the superconducting state. According to our results in the underdoped sample (Fig. 7), $\Delta W/W_s = 0.65 \pm 0.18$ at 1 eV, which yields $\Delta E_k = 1.1 \pm 0.3$ meV per copper site. This would be a huge kinetic energy gain, ~ 15 times larger than the condensation energy U_0. For optimally doped Bi-2212, $U_0 \simeq 1$ J/g-at ≈ 0.08 meV per copper site.[30] A change of the in-plane kinetic energy could actually drive the superconducting transition, as it has been proposed in various scenarios: holes moving in an antiferromagnetic background,[31–33] interlayer tunneling theory,[34] or hole undressing.[10,11,14] The latter scenario suggests that the violation of the FGT sum rule must be more conspicuous for a dilute concentration of carriers and that, upon doping, a conventional energy scale exhausting the FGT sum-rule should be retrieved. A more recent scenario, based on the changes of the momentum distribution function (rather than on changes of the carrier mass) when entering the superconducting state, also explains semi-quantitatively our data.[16]

A comparison of the IR and visible-ultraviolet changes of spectral weight is an interesting check of the self consistency of our data. As the total spectral weight, when integrating from zero to infinity, should be conserved regardless of the variation of any external parameter (*e.g.*, temperature), one can write:

$$\int_0^{1\ \mathrm{eV}/\hbar} \Delta\sigma_1(\omega)d\omega = -\int_{1\ \mathrm{eV}/\hbar}^{\infty} \Delta\sigma_1(\omega)d\omega \approx \int_{1\ \mathrm{eV}/\hbar}^{3\ \mathrm{eV}/\hbar} -\Delta\sigma_1(\omega)d\omega \tag{3}$$

Δ stands for a temperature variation. Assuming that the temperature variations of the spectral weight (of the conductivity thereof) beyond ~ 3 eV can be neglected, the temperature changes in kinetic energy, that are directly related to the left integral in Eq. 3, can be approximated as well from the right integral. The results of this calculation for the underdoped sample are shown in Figure 9, together with the calculation from the left integral. The integral from 1 to 3.1 eV is subject to larger uncertainties as it is calculated *only* in the high frequency range, which is more affected by the proximity of the highest experimental frequency cut-off, resulting in more scatter in fig.9. The integral up to 1 eV is much less affected since it is calculated well below this highest experimental frequency cut-off. There is a reasonable agreement between the IR and the visible-ultraviolet changes of spectral weight. Figure 9 shows the jump of about 1 meV at the superconducting transition. Note however that while the changes in spectral weight deduced from the visible-ultraviolet regime indicate that there is an "extra" transfer of spectral weight to the IR region at the superconducting transition,[15] it is the analysis of the IR spectral weight *and* of the superfluid weight that actually tells that such extra transfer is used to build-up the superconducting condensate (Fig. 7).

Recently, STM experiments in optimally doped Bi-2212 samples showed small scale spatial inhomegeneities, over $\simeq 14$ Å, which are reduced significantly when doping increases, and whose origin could be local variations of oxygen concentration.[35] Since the wavelength in the full spectral range is larger than 14 Å, the reflectivity performs a large scale average of such an inhomogeneous medium. The implications in the conductivity are still to be investigated in detail, but it is presently unclear how this could affect the sum rule.

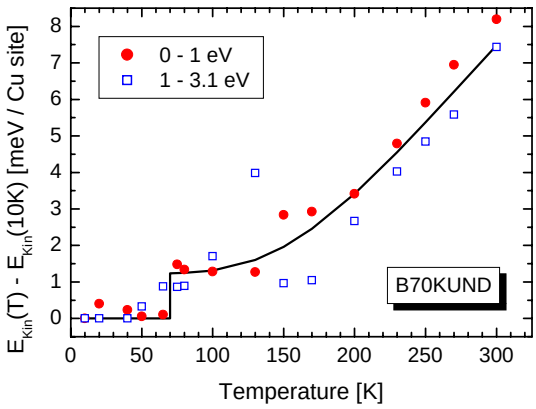

Figure 9. Temperature changes in kinetic energy per charge carrier, as calculated from the infrared (full circles) and visible-ultraviolet (open squares) changes in spectral weight (see Eq. 3). The kinetic energy at 10 K is taken as the ground energy. The 1 eV frequency cut-off can be changed from 0.8 to 1.2 without altering the main features (in particular the 1 meV jump at T_c). The line is a guide for the eye.

5. CONCLUSIONS

In conclusion, we have have found for the in-plane conductivity of the underdoped Bi-2212 a clear violation of the FGT sum rule at 1 eV, corresponding to a large ($\sim$ 30 %) transfer of spectral weight from regions of the visible-ultraviolet spectrum to the superfluid condensate. Within the framework of the tight-binding Hubbard model, this corresponds to a kinetic energy lowering of $\sim$ 1 meV per copper site. The very large energy scale required in order to exhaust the sum rule in the underdoped sample cannot be related to a conventional bosonic scale, hence strongly suggests an electronic pairing mechanism.

ACKNOWLEDGMENTS

We are very grateful to M. Norman and C. Pépin for illuminating discussions. We acknowledge fruitful comments from J. Hirsch and E.Ya. Sherman. We thank P. Dumas (LURE, Orsay) for his help with the IR microscopy measurements. AFSS thanks Colciencias and Ministère Français des Affaires Etrangères (through the Eiffel Fellowships Program) for financial support. RPSML acknowledges the financial support of CNRS-ESPCI.

REFERENCES

1. T. Timusk and D. Tanner in *Physical Properties of High-Temperature Superconductors*, D. Ginsberg, ed., **I**, pp. 339–407, World Scientific, Singapore, 1989.
2. D. Tanner and T. Timusk in *Physical Properties of High-Temperature Superconductors*, D. M. Ginsberg, ed., **III**, pp. 363–469, World Scientific, Singapore, 1989.
3. R. A. Ferrell and R. E. Glover *Phys. Rev.* **109**, p. 1398, 1958.
4. M. Tinkham and R. A. Ferrell *Phys. Rev. Lett.* **2**, p. 331, 1959.
5. C. Renner, B. Revaz, J. Y. Genoud, K. Kadowaki, and O. Fischer *Phys. Rev. Lett.* **80**, p. 149, 1998.
6. M. Randeria and J. C. Campuzano *cond-mat/9709107* , 1997.
7. D. N. Basov, S. I. Woods, A. S. Katz, E. J. Singley, R. C. Dynes, M. Xu, D. G. Hinks, C. C. Homes, and M. Strongin *Science* **283**, p. 49, 1999.
8. A. S. Katz, S. I. Woods, E. J. Singley, T. W. Li, M. Xu, D. G. Hinks, R. C. Dynes, and D. N. Basov *Phys. Rev. B.* **61**, p. 5930, 2000.
9. D. N. Basov, C. C. Homes, E. J. Singley, M. Strongin, T. Timusk, G. Blumberg, and D. van der Marel *Phys. Rev. B* **63**, p. 134514, 2001.
10. J. E. Hirsch *Physica C* **199**, p. 305, 1992.

11. J. E. Hirsch *Physica C* **201**, p. 347, 1992.
12. J. E. Hirsch and F. Marsiglio *Physica C* **331**, p. 150, 2000.
13. J. E. Hirsch and F. Marsiglio *Phys. Rev. B* **62**, p. 14487, 2000.
14. J. E. Hirsch and F. Marsiglio *Phys. Rev. B* **62**, p. 15131, 2000.
15. H. J. A. Molegraaf, C. Presura, D. van der Marel, P. H. Kes, and M. Li *Science* **295**, p. 2239, 2002.
16. M. R. Norman and C. Pépin *cond-mat/0201415* , 2002.
17. Z. Z. Li, S. Labdi, A. Vaures, S. Megtert, and H. Raffy in *Proceedings of the Symposium A1 of the ICAM 91-EMRS*, L. Correa, ed., p. 487, Elsevier, New York, 1992.
18. Z. Konstantinovic, Z. Z. Li, and H. Raffy *Physica B* **259-261**, p. 569, 1999.
19. Z. Konstantinovic *PhD Thesis, Université de Paris-Sud (unpublished)* , 2001.
20. E. G. Maksimov, H. J. Kaufmann, E. K. H. Salje, Y. de Wilde, N. Bontemps, and J. P. Contour *Solid State Commun.* **112**, p. 449, 1999.
21. D. van der Marel, H. J. A. Molegraaf, C. Presura, M. Grueninger, and B. Dam, "Optical signatures of electron correlations in the cuprates," in *Lecture notes, Trieste miniworkshop "Strong correlation in the high T_c era"*, ICTP, Trieste, 17-28 July 2000.
22. F. A. Polack, R. Mercier, L. Nahon, C. Armellin, J. P. Marx, M. Tanguy, M. E. Couprie, and P. Dumas in *SPIE Proceedings on Accelerator-Based Sources of Infrared and Spectroscopic Applications*, G. L. Carr and P. Dumas, eds., **3775**, pp. 13–21, SPIE, 1999.
23. M. J. Holcomb *Phys. Rev. Lett.* **73**, p. 2360, 1994.
24. W. A. Little, K. Collins, and M. J. Holcomb *J. Supercond.* **12**, p. 89, 1999.
25. M. A. Quijada, D. B. Tanner, R. J. Kelley, M. Onellion, H. Berger, and G. Margaritondo *Phys. Rev. B* **60**, p. 14917, 1999.
26. A. F. Santander-Syro, R. P. S. M. Lobo, N. Bontemps, Z. Konstantinovic, Z. Z. Li, and H. Raffy *Phys. Rev. Lett.* **88**, p. 097005, 2002.
27. G. Villard, D. Pelloquin, and A. Maignan *Phys. Rev. B* **58**, p. 15231, 1998.
28. D. D. Castro, N. L. Saini, A. Bianconi, and A. Lanzara *Physica C* **332**, p. 405, 2000.
29. S. Chakravarty *Eur. Phys. J. B* **5**, p. 337, 1998.
30. J. W. Loram, J. L. Luo, J. R. Cooper, W. Y. Liang, and J. L. Tallon *Physica C* **341-348**, p. 831, 2000.
31. J. Bonca, P. Prelovsek, and I. Sega *Phys. Rev. B* **39**, p. 7074, 1989.
32. E. Dagotto, J. Riera, and A. P. Young *Phys. Rev. B* **42**, p. 2347, 1990.
33. T. Barnes, A. E. Jacobs, M. D. Kovarik, and W. G. Macready *Phys. Rev. B* **45**, p. 256, 1992.
34. P. W. Anderson *Science* **258**, p. 1154, 1995.
35. S. H. Pan, J. P. O'Neal, R. L. Badzey, C. Chamon, H. Ding, J. R. Engelbrecht, Z. Wang, H. Eisaki, S. Uchida, A. K. Gupta, K.-W. Ng, E. W. Hudson, K. M. Lang, and J. C. Davis *Nature* **413**, p. 282, 2001.